Direct detection of wavelike spatial structure at the bottom of the F region and its role on the formation of equatorial plasma bubble

A. K. Patra,[1] A. Taori,[1] P. P. Chaitanya,[2] and S. Sripathi[3]

Received 23 July 2012; revised 23 January 2013; accepted 23 January 2013; published 4 March 2013.

[1] We present hitherto unrevealed wavelike spatial structures, as seen in the 630 nm airglow intensity using a scanning photometer, prior to the occurrence of equatorial plasma bubble (EPB). The dominant wavelengths in the spatial variation of airglow intensity have excellent correspondence with the spatial separations of periodic plume structures in the radar observations, and the amplitudes of the wave perturbations (6–12%) are significantly more than the commonly quoted 5% seed perturbation used in simulation studies. In contrast, no such airglow structure was observed on EPB free evening. Concurrent ionosonde observations made from the magnetic equator, although displayed satellite trace on some occasions, did not show one-to-one correspondence between the occurrence of satellite trace and EPB, a finding that is inconsistent with a recent suggestion that satellite trace can be used as a precursor of EPB occurrence. The new findings are discussed in the light of current understanding of the day-to-day variability in EPB including its prediction.

Citation: Patra, A. K., A. Taori, P. P. Chaitanya, and S. Sripathi (2013), Direct detection of wavelike spatial structure at the bottom of the F region and its role on the formation of equatorial plasma bubble, *J. Geophys. Res. Space Physics*, *118*, 1196–1202, doi:10.1002/jgra.50148.

1. Introduction

[2] The day-to-day variability in the occurrence of equatorial plasma bubble (EPB)/equatorial spread F (ESF), a vital component of the ionospheric weather, continues to puzzle the equatorial aeronomers. An associated essential constituent, yet unknown on a given evening, is the presence of the required seed perturbation for the initiation of the Rayleigh-Taylor (RT) instability forming the EPB. Atmospheric gravity waves (AGW) are believed to provide the required seed perturbation [*Fritts et al*., 2008, and references therein], but due to the difficulties in measuring the AGW parameters at the bottom of the F region, its role in seeding EPB is yet to be established satisfactorily. In the recent time, emphasis was made on the role of large-scale wave structures (LSWS) [*Tsunoda and White*, 1981] in the day-to-day variability of EPB occurrence [*Tsunoda*, 2005]. This particular proposal is inspiring since observation and theoretical modeling strongly suggest that the shear flow in the post-sunset F region [*Kudeki and Bhattacharyya*, 1999] is capable of forming LSWS on its own through collisional shear instability [*Hysell and Kudeki*, 2004]. The detection of LSWS in question, however, was made only by the ALTAIR radar, an incoherent scatter radar (ISR) with scanning capability [*Tsunoda and White*, 1981]. Due to the paucity of such ISR at other longitudes, satellite trace (ST) in ionogram was used as proxy of LSWS and some case studies suggested that ST can be used as a precursor of EPB [*Tsunoda*, 2008]. Others found that there exist cases showing no relationship between ST and EPB [*Narayanan et al*., 2012; *Li et al*., 2012], suggesting that the mere occurrence of ST cannot be considered as a reliable predictor of EPB occurrence. It is not surprising since the presence of ST alone is not sufficient to describe the much required zonal wavelength and perturbation amplitude of the LSWS in question. Importantly, *Makela and Miller* [2008] showed that the presence of LSWS alone is not sufficient for the growth of the RT instability, implying that any LSWS may not serve as a suitable seed perturbation for the EPB growth. Total electron content variations from ground-based reception of radio beacon signal from C/NOFS, an equatorial orbiting satellite, have also been used to get such signature [e.g., *Thampi et al*., 2009], but such observations are difficult to obtain as required for addressing the day-to-day variability of EPB due to limited satellite overpass. Given the fact that ISR of the type of ALTAIR radar is highly expensive, efforts will continue to be made to utilize the relatively inexpensive instruments to detect the seed perturbation required for the growth of EPB.

[3] In this paper, we demonstrate, for the first time, an inexpensive yet unique technique, based on airglow photometry, providing the precursor wave features, such as the zonal wavelength and perturbation amplitude, and an exceptionally close correlation between these and the EPB occurrence. Importantly, these wavelike features were detected well before the onset of EPB and in some cases before the F region sunset. We also demonstrate how these wave structures eventually manifested in the radar observations of EPB-related plumes. These new findings are finally discussed in the light of

[1]National Atmospheric Research Laboratory, Gadanki, India.
[2]Department of Physics, S V University, Tirupati, India.
[3]Indian Institute of Geomagnetism, Navi Mumbai, India.

Corresponding author: A. K. Patra, National Atmospheric Research Laboratory, Gadanki, India. (akpatra@narl.gov.in)

2169-9380/13/10.1002/jgra.50148

the prevailing LSWS/AGW seeding hypotheses of the RT instability governing the day-to-day variability of EPB occurrence.

2. Experiment

[4] The key observations that provided unprecedented characteristics of seed perturbation for EPB formation were made from Gadanki (13.5°N, 79.2°E, 6.5°N mag. lat) by scanning an airglow photometer, operated at 630 nm, in the east-west plane [*Taori et al.*, 2011]. In the present study, scanning was performed from 30°E to 30°W from zenith (within which the difference in Van-Rhjin effect is <2%) at each 5° interval. Thus, the observations are representative of zonally varying airglow intensity at an altitude of ~250 km and spanning over a horizontal extent of ~288 km. Considering that the altitude of airglow could vary by ±25 km (i.e., 250 ± 25 km), the horizontal extent could vary by ±28 km (i.e., 288 ± 28 km). At every position, photon counts were integrated for 20 s. Although at each position the photometer took 20 s for making measurement, it took 11 min to complete one full scan due to slow movement of the steppered motor attached to the scanning assembly in order to maintain stability while changing the look angle. On average, we carried out three scans on each evening soon after the sunset and prior to the onset of EPB (as seen by the Gadanki MST radar). On a few nights, we continued the photometer observations but only in the zenith direction. It may be important to mention that the ionospheric region at an altitude of ~250 km over Gadanki is connected to 350 km over the magnetic equator via the magnetic field lines, and thus, the perturbation in airglow observations is of practical significance. Overhead occurrence of EPB including their morphological features was characterized using the Gadanki MST radar observations of F region field-aligned irregularities (FAI). Radar observations of the F region FAI from the height region of 84–684 km were made with a range resolution of 2.4 km, time resolution of 30 s, unambiguous velocity limit of ±283 m s^{-1}, and velocity resolution of 2.28 m s^{-1} [for similar measurements, refer to *Patra et al.*, 2009]. Also, ionosonde observations were made from a magnetically equatorial station Tirunelveli (8.5°N, 78.2°E, 0.5°N mag. lat) to monitor the F layer height, ESF, and ST.

3. Observational Results

[5] We carried out radar and airglow observations during February–March 2012 to examine spatial wavelike structures, if any, in the airglow observations prior to the onset of EPB. Radar observations were carried out on 19 nights, and EPB was observed on 16 nights. Airglow observations were carried out on eight nights when clear-sky condition prevailed. Out of eight nights of simultaneous observations, EPB was observed on six nights. Significant spatial variation in the airglow intensity was observed prior to the occurrence of EPB on all the EPB events (i.e., six nights), and no such variation was observed on the evening of non-EPB events. In the following, we present a few case studies, which include three EPB and one non-EPB events, to demonstrate the role of the observed seed structures on the onset of EPB.

3.1. Observations Related to EPB Event

[6] Three examples of EPB events observed on 19, 20, and 26 March 2012 by the Gadanki radar and the Tirunelveli ionosonde are shown in Figures 1a–1c and 1d–1f,

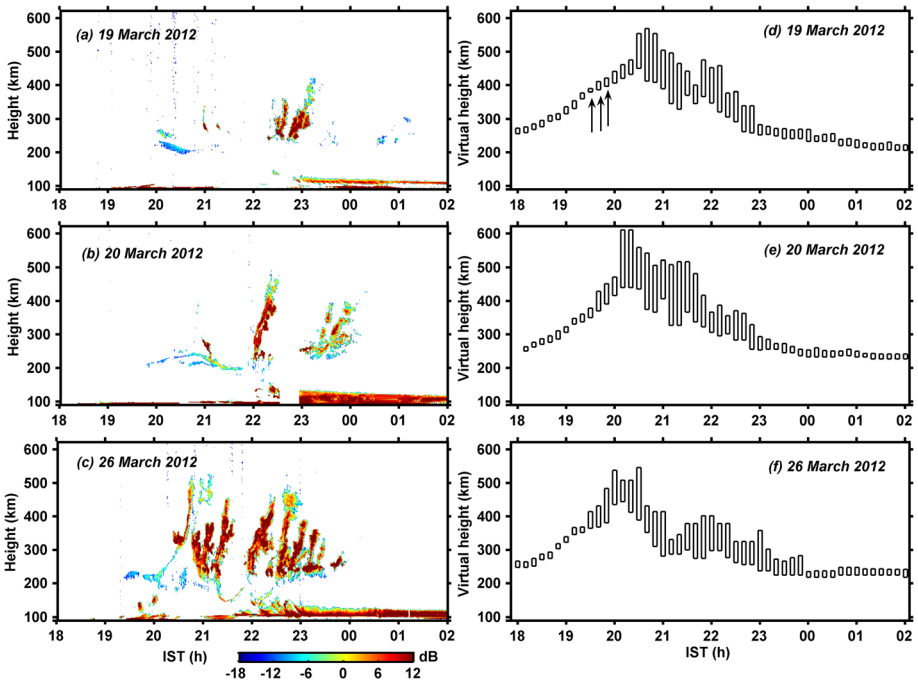

Figure 1. Height-time variation of radar echo SNR from the F region irregularities observed from Gadanki on (a) 19 March, (b) 20 March, and (c) 26 March 2012. Ionosonde observations, displaying h′F and range type ESF observed from Tirunelveli on (d) 19 March, (e) 20 March, and (f) 26 March 2012. The upward directed arrows in Figure 1d represent the occurrence of ST at those times.

respectively. The height-time SNR maps shown in Figures 1a–1c clearly portray the plume structures representing EPB observed on the three nights. F region sunset occurred at 19:35 IST (Indian Standard Time = UT + 5.5 h), and while the bottomside echoes commenced soon after the sunset, the plumes commenced during 20:30–21:00 IST. In all the three events, the bottomside band structures were located around 250 km altitude. On 19 and 20 March, the initial plumes, which occurred at ~21:00 IST, were not so well developed, as compared to that of 26 March, when they were over the radar site. On 19 March, one can clearly notice that a pair of plumes, separated by ~30 min, occurred at ~21:00 IST, and after ~1 h, another pair of plumes, again separated by ~30 min, occurred. After 23:30 IST, some plume structures can also be noted, but they appear to be in their decay phases and hence are not as clear as those observed before 23:30 IST. On 20 March, the time gap between the plumes was also ~1 h but the plumes did not occur in pair. On 26 March, however, the plume separation was 20–30 min. Assuming that the plume structures moved across the radar beam with a background zonal drift, the temporal structures of the plumes in the slit camera mode of radar observations can be approximately translated into zonal structures. Taking zonal drifts as 80 m s^{-1}, which is quite realistic after 21:00 IST corresponding to low/moderate solar activity condition [*Kumar et al*., 1995], the plume recurrence periods of 30 min and 1 h could be viewed as plume structures with spatial spacing of 144 and 288 km.

[7] Figures 1d–1f show ionosonde observations of the F region echoes from Tirunelveli, a magnetic equatorial station located close to the longitude of Gadanki. The base and the vertical extent of each box represent virtual height of the F layer base (h′F) and the range type ESF, respectively. When ESF is present, they represent the bottom and top height of the ESF echoes. It is interesting to note that the durations of ESF echoes and radar plumes were in reasonably good agreement. On all the three evenings, prior to the occurrence of radar plumes/ESF, h′F was ≥350 km. It is important to mention that ST was observed only on 19 March during 19:30–19:50 IST, which are shown as upward directed arrows in Figure 1d.

[8] Coming to the airglow observations, we begin with a detailed presentation of the 19 March event, for which we have observations from 19:19 IST unlike other events which were started at ~19:30 IST, to examine local time and look angle effects on the airglow intensity and also the relationship of the airglow depletions with the radar plumes. Figure 2 shows scanning photometer observations at 630 nm made at three time periods, one after the other, prior to the occurrence of radar plume on 19 March. Observations were made from 30°E to 30°W, and the results are plotted with positive (negative) x axis representing east (west) with respect to Gadanki. Note that observations corresponding to the 30°E position are not shown since they were affected by the street light. The most important aspect of these observations is the noticeable spatial variations in the airglow intensity displaying wavelike pattern. One can also note that the level of airglow intensity varies from one scan to the other, indicating decreasing level of airglow intensity with time. No significant change in the airglow intensity with look angle, however, was noticed.

[9] Figure 3 shows local time variation of airglow intensity in the vertical direction. Three data points prior to 20:00 IST correspond to vertical observations in the three scan cycles. A decreasing pattern in the airglow intensity is clearly evident. Superposed over this decreasing trend, one can note periodic depletions in airglow observations having close

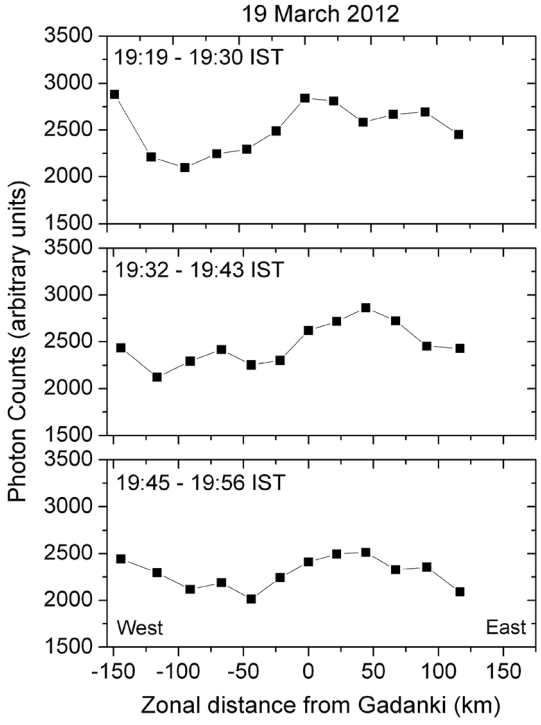

Figure 2. Airglow intensity (630 nm) as a function of zonal distance observed using a scanning photometer from Gadanki on 19 March 2012. Three panels represent observations made at three different time periods during 19:19–19:56 IST.

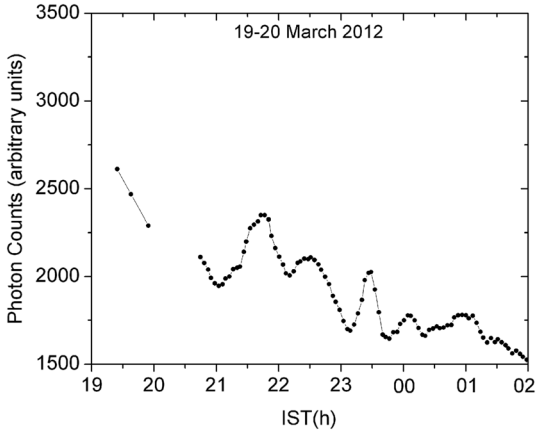

Figure 3. Local time variation of 630 nm airglow intensity in the vertical direction observed from Gadanki on 19 March 2012. Three data points prior to 20:00 IST correspond to vertical observations in the three scan cycles made during 19:19–19:56 IST.

correspondence with the plumes observed in the radar observations (shown in Figure 1a).

[10] In order to illustrate the wave signatures clearly and their relationship to the plume structures shown in Figure 1, we present perturbation amplitude in the airglow intensity variation (obtained after subtracting the mean) as a function of zonal distance in Figures 4a–4c, respectively. Again, the three panels represent observations made at three different time periods, one after the other, prior to the occurrence of radar plume. Dashed lines represent best fit cosine model revealing the dominant wavelengths. In all the three events, remarkable wave signature can be noted. Also from successive scans, we found that the structures were either stationary or slowly drifting, implying that horizontal wavelength can be estimated with reasonable accuracy. The primary wavelengths, estimated from the best fit curve, corresponding to 19, 20, and 26 March are 230, 280, and 144 km, respectively. Corresponding perturbation amplitudes in terms of percentage are 12%, 11%, and 12%, respectively. Note that on 26 March, the primary wavelength is nearly half of those of 19 and 20 March. It is interesting to recall that the periodic plume structures, as seen in the radar observations, were much closely spaced on 26 March compared to those observed on 19 and 20 March. Thus, at the first look, the correspondence between the radar and airglow observations is quite appealing and the observed airglow structures should be considered significant for studying the occurrence of EPB. Further, these wavelike structures were clearly observed 1–1.5 h before the occurrence of the radar plumes.

[11] From successive scans, we infer that the wave structures were either stationary or slowly drifting in the westward direction (on 26 March), implying that the altitude of the airglow intensity (which is ~250 km) was at the near-zero zonal velocity zone of the shear flow or just below that, where the flow is westward [*Kudeki and Bhattacharyya*, 1999]. From successive scans, which were made over a time period of ~40 min, we, however, do not find any noticeable enhancement in the wave amplitude.

[12] The presence of shorter scale wave structures, in the form of deviations from the best fit model data, can also be inferred. To find out various dominant wave components involved in the airglow observations, we performed the best fit analysis on all the airglow data that we have, and the wavelengths and corresponding perturbation amplitudes for the EPB events are summarized in Table 1. Estimation errors in the wavelength linked with the best fit analysis are also shown. The primary and secondary waves were in the range of 90–300 km and 80–240 km, respectively, and percentage amplitudes are in the range of 6–12%. On 17 March, an additional wave component having wavelength of 215 km and wave amplitude of 6% was observed.

3.2. Observations Related to Non-EPB Event

[13] Figures 5a–5c display the radar, ionosonde, and airglow observations, respectively, corresponding to a non-EPB event of 22 February 2012. The upward directed arrows in Figure 4b represent the occurrence of ST at those times. As is evident from Figures 4a and 4b, no plume was observed by the Gadanki radar and no ESF was noticed at Tirunelveli. Note that on this evening h′F was ~350 km, which was very much similar to those of 19, 20, and 26 March, and ST was also observed during 19:20–19:40 IST, but EPB/ESF did not occur.

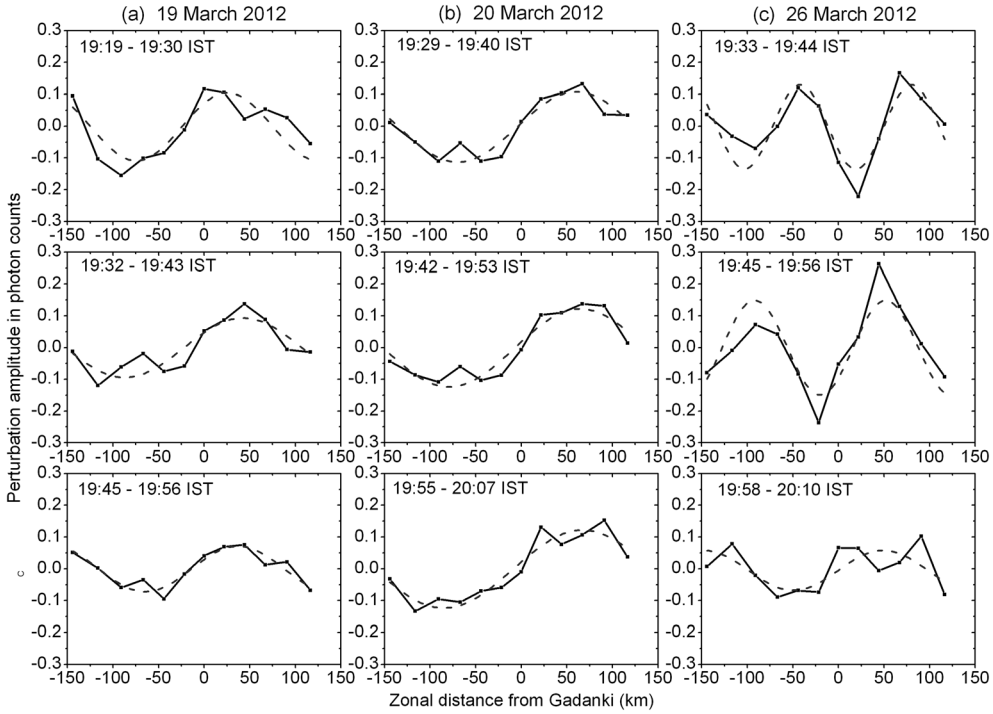

Figure 4. Airglow intensity variations (630 nm) (after subtracting the mean) as a function of zonal distance observed using a scanning photometer from Gadanki on (a) 19 March, (b) 20 March, and (c) 26 March 2012. Three panels represent observations made at three different time periods. Dashed lines represent the best fit curve corresponding to the primary wavelength.

Table 1. Dominant Horizontal Wavelengths and Corresponding Perturbation Amplitudes Estimated Using Best Fit Analysis

Date	Dominant Horizontal Wavelength (km) ± Error	Perturbation Amplitude (%)
27 February 2012	103 ± 25	12.0
	240 ± 30	6.0
17 March 2012	90 ± 11	10.0
	140 ± 15	8.0
	215 ± 22	6.0
19 March 2012	230 ± 30	12.0
	80 ± 21	7.0
20 March 2012	280 ± 35	11.0
	108 ± 18	8.0
24 March 2012	300 ± 40	9.0
	122 ± 29	6.0
26 March 2012	144 ± 19	12.0
	92 ± 20	10.0

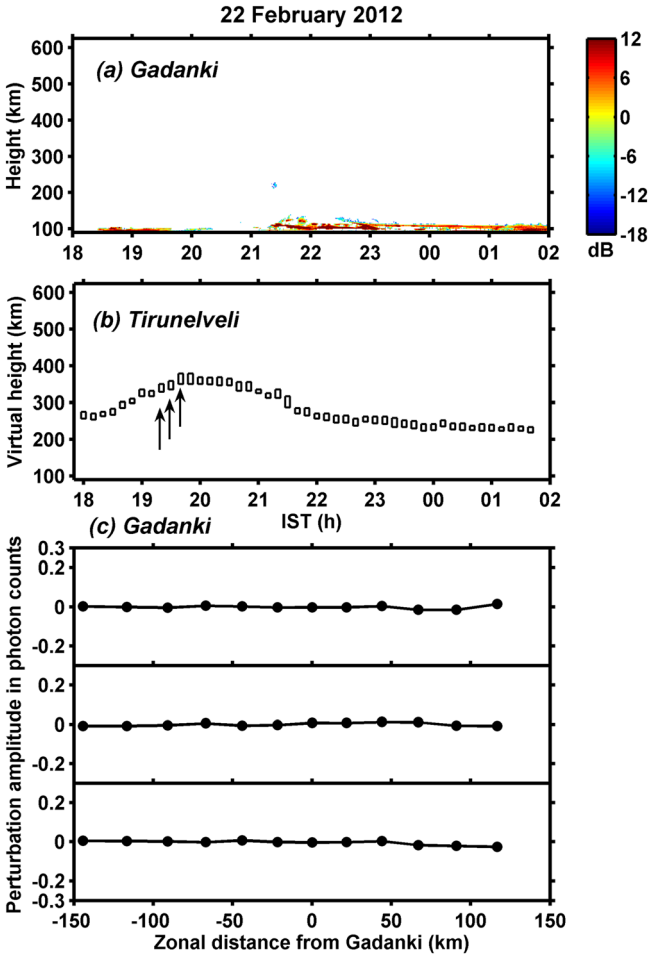

Figure 5. (a) Height-time variation of radar echo SNR observed from Gadanki, (b) ionosonde observations, displaying h′F/ESF echoes observed from Tirunelveli, and (c) 630 nm airglow observations at three time durations corresponding to a non-EPB event of 22 February 2012. The upward directed arrows in Figure 5b represent the occurrence of ST at those times.

Interestingly, on this evening, the airglow observations made at all the three time durations also showed no noticeable intensity variations unlike those observed on 19, 20, and 26 March. The best fit analysis performed on the airglow observations reveals that the perturbation amplitudes are ≤0.5%. On another non-EPB night (27 March 2012) also, the perturbation amplitudes were found to be ≤0.8%.

4. Discussion and Concluding Remarks

[14] Important new results are as follows: (1) detection of wavelike structures in the 630 nm airglow intensity well before the occurrence of EPB and no such structure associated with EPB free evening, (2) exceedingly well correspondence between the dominant wavelengths in the airglow intensity variations and the spatial separations of the periodic plume structures, and (3) amplitudes of the wave perturbations in the range of 6–12% linked with the EPB events and their potential in seeding EPB.

[15] Intriguingly, we also found no one-to-one correspondence between the occurrence of ST and EPB, a finding that suggests that the mere presence of ST cannot be taken as a precursor of EPB. This finding is in agreement with the finding recently reported by *Narayanan et al*. [2012] and *Li et al*. [2012]. *Makela and Miller* [2008] also showed that zero, one, or multiple depletions could occur on large-scale wave structures, implying that large-scale wave structure is not sufficient for the growth of EPB. Thus, it looks that while the ST can be used as a signature of wavy electron density structure, associated wavelength and perturbation amplitude cannot be obtained. For example, if the wavelength is too large (say, >600 km) and there is a lack of spatial resonance [*Kelley et al*., 1981] or absence of shorter wave structure (say, ~200 km wavelength), it is unlikely that the RT instability would grow [*Sekar et al*., 2001].

[16] While an unprecedented correspondence between the spatial structures in the airglow and plumes spacings was found, it is also important to note that the dominant wavelengths varied widely from one night to other. The primary and secondary waves were in the range of 90–300 km and 80–240 km, respectively. We also found that an additional wave component with wavelengths of 215 km was present on 17 March. It is interesting to note that on 26 March, the primary wavelength is nearly half of those of 19 and 20 March, and plume activities were much more violent than those on 19 and 20 March. Also, on 26 March, we noted westward drift in the airglow structures unlike those on 19 and 20 March. Considering that the zonal plasma flow in the evening equatorial ionosphere has a shear, westward below and eastward above, the westward drift of the structures on 26 March implies that the airglow layer (which is at ~250 km) was in the region of westward flow, and on the same logic on 19 and 20 March, they were possibly close to the shear node, where the flow is near zero. This being the case, it is quite likely that the observed structures, having wavelength of 144 km and large perturbation amplitude (12%), on 26 March were linked with the shear-driven instability [*Hysell and Kudeki*, 2004]. This, however, does not eliminate that the wave structures observed on 19 and 20 March cannot be associated with the same instability. Considering that the wavelengths (140 and 275 km) and height region both agree well with those expected from the theory of *Hysell and Kudeki* [2004], the large amplitude perturbation observed on 26 March suggests that the

westward drifting strata possibly stimulate the instability growth better at lower altitudes than at higher altitudes.

[17] While the above arguments fit well with those expected from the shear instability [*Hysell and Kudeki*, 2004], there lies equal possibility for the AGW, too. *Makela et al*. [2010] found that the EPB spacings were consistent with the dominant AGW wavelength of ~200 km [*Vadas and Crowley*, 2010], suggesting a connection between the AGW and EPB seeding. Since AGW having wavelength <400 km can propagate to the F region [*Vadas*, 2007] and the wavelength of the airglow perturbations reported here are in the range of 40–300 km, both shear-driven LSWS and AGW should be considered plausible. The relative merit of these on a given evening, however, could vary, which needs experimental verification. As far as the shear-driven LSWS in the long wavelength regime is concerned, the predicted wavelength is ~200 km [*Hysell and Kudeki*, 2004], and thus for a given shear scale, a particular wavelength in the long wavelength regime is expected to grow. The observations, however, show multiple wavelengths on a given evening, which suggest that both LSWS and AGW could coexist and play important roles in seeding EPB.

[18] Thus, while the origin of these structures continues to be a subject of further investigations, we must stress that unambiguous detection of the wave structures of the type shown here would be of practical relevance in understanding the day-to-day variability of EPB occurrence and also in its prediction. Especially, detection of the wavelike structures at least 1–1.5 h prior to the first sighting of radar plumes can be used for the possible prediction of the EPB occurrence. *Makela and Miller* [2008] also studied the day-to-day variability of EPB using airglow imager observations made mostly after 20:00 LT. They, however, did not focus on the wavelike variations, which have predictive possibility for the onset of EPB of the type shown in the present work. An important issue of detecting these structures, however, lies in the 630 nm airglow intensity, which maximizes at an altitude of ~250 km. Since the equatorial F region would be at a higher altitude due to upward movement of the F layer till sunset, low latitude locations would be most suited for such measurement.

[19] Having shown that the wavelike spatial structures in the 630 nm airglow observations had striking correspondence with the EPB occurrence and their characteristics, one aspect that remains to be understood is whether the spatial structures in airglow could be interpreted as seed perturbation or structures associated with the initial stage of EPB growth. From the airglow observations, it was clear by ~19:40 IST whether or not wavelike structures were present on a given night. We also note from Figures 1d–1f and 5c that during 19:00–19:40 IST, h′F at the magnetic equator were near identical irrespective of the occurrence of EPB. The amplitudes of the wave structures in 630 nm airglow were in the range of 6–12% corresponding to the EPB events, while those corresponding to non-EPB events were only 0.5–0.8%. Assuming that the behavior of the bottomside F region did not vary significantly within a few minutes of the scanning period, as inferred from h′F data (in Figures 1d–1f and 5c), the perturbation amplitudes of airglow intensity may be considered as a rough proxy of electron density perturbations. This, however, by no means implies that the airglow intensity can be simply translated into electron density. This needs in-depth investigation, which is beyond the scope of the present work. Under the assumption mentioned above, the observed perturbation amplitudes appear to be more than the commonly used 5% perturbation in electron density for seeding EPB [e.g., *Zalesak et al*., 1982]. This, however, needs further investigation. In the above context, if we were to interpret these structures as signatures of initial stage of EPB growth, we would expect amplitude of the airglow perturbation to increase with time. We, however, have not observed such amplitude enhancement in the successive scans. On the other hand, airglow intensity observed at a later time clearly shows deep bite out having excellent correlation with the radar plumes. On 19 March, airglow observation could be started at 19:19 IST, and we could clearly notice the presence of the wave structures at that time. On this evening, when the F layer height at equatorial location Tirunelveli was in the rising phase, the airglow structures were observed at Gadanki prior to the occurrence of ST and subsequent spread F at Tirunelveli and also well before the occurrence of plume structures at Gadanki. Thus, although it is clear that the wave structures were observed well before the bubble occurrence, in the absence of similar airglow observations from equatorial station Tirunelveli, it may be difficult to unambiguously say whether they were the seed perturbation. Further investigation would be required to clarify this aspect.

[20] In closing, we should reiterate that the observations on wavelike spatial structures having close linkage with the occurrence and characteristics of EPB are significant new results and such structures can be detected using inexpensive scanning photometer from other longitude sectors to test their potential in understanding the day-to-day variability of EPB. How well in advance these structures can be detected is another issue that needs to be examined. Efforts are being made to develop a large data base to establish the aforementioned linkage on a statistical basis and also the early detection of these structures.

[21] **Acknowledgment.** The authors gratefully acknowledge NARL technical staff for making the observations reported here.

References

Fritts, D. C., et al. (2008), Gravity wave and tidal influences on equatorial spread F based on observations during the Spread F Experiment (Spread FEx), *Ann. Geophys.*, *26*, 3235–3252, doi:10.5194/angeo-26-3235-2008.

Hysell, D. L., and E. Kudeki (2004), Collisional shear instability in the equatorial F region ionosphere, *J. Geophys. Res.*, *109*, A11301, doi:10.1029/2004JA010636.

Kelley, M. C., M. F. Larsen, C. LaHoz, and J. P. McClure (1981), Gravity wave interaction of equatorial spread F: A case study, *J. Geophys. Res.*, *86*, 9087–9100.

Kudeki, E., and S. Bhattacharyya (1999), Post-sunset vortex in equatorial *F* region plasma drifts and implications for bottomside spread-F, *J. Geophys. Res.*, *104*, 28163–28170.

Kumar, S., A. K. Gwal, B. M. Pathan, and D. R. K. Rao (1995), Zonal drifts of ionospheric irregularities at temperate latitude in the Indian region, *Ann. Geophys.*, *13*, 724–729.

Li, G., B. Ning, M. A. Abdu, W. Wan, and L. Hu (2012), Precursor signatures and evolution of post-sunset equatorial spread F observed over Sanya, *J. Geophys. Res.*, *117*, A08321, doi:10.1029/2012JA017820.

Makela, J. J., and E. S. Miller (2008), Optical observations of the growth and day-to-day variability of equatorial plasma bubbles, *J. Geophys. Res.*, *113*, A03307, doi:10.1029/2007JA012661.

Makela, J. J., S. L. Vadas, R. Muryanto, T. Duly, and G. Crowley (2010), Periodic spacing between consecutive equatorial plasma bubbles, *Geophys. Res. Lett.*, *37*, L14103, doi:10.1029/2010GL043968.

Narayanan, V. L., A. Taori, A K Patra, K. Emperumal, and S. Gurubaran (2012), On the importance of wave-like structures in the occurrence of

equatorial plasma bubbles: A case study, *J. Geophys. Res.*, *117*, A01306, doi:10.1029/2011JA017054.

Patra, A. K., D. V. Phanikumar, and T. K. Pant (2009), Gadanki radar observations of F region field-aligned irregularities during June solstice of solar minimum: First results and preliminary analysis, *J. Geophys. Res.*, *114*, A12305, doi:10.1029/2009JA014437.

Sekar, R., E. A. Kherani, P. B. Rao, and A. K. Patra (2001), Interaction of two long-wavelength modes in the nonlinear numerical simulation model of equatorial spread F, *J. Geophys. Res.*, *106*, 24,765–24,775.

Taori, A., N. Dashora, K. Raghunath, J. M. Rusell III, and M. G. Mlynczak (2011), Simultaneous mesosphere, thermosphere-ionosphere parameter measurements over Gadanki (13. 5^{o} N, 79.2^{o} E)- First results, *J. Geophys. Res.*, *116*, A07308, doi:10.1029/2010JA016154.

Thampi, S. V., M. Yamamoto, R. T. Tsunoda, Y. Otsuka, T. Tsugawa, J. Uemoto, and M. Ishii (2009), First observations of large-scale wave structure and equatorial spread F using CERTO radio beacon on the C/NOFS satellite, *Geophys. Res. Lett.*, *36*, L18111, doi:10.1029/2009GL039887.

Tsunoda, R. T. (2005), On the enigma of day-to-day variability in equatorial spread F, *Geophys. Res. Lett.*, *32*, L08103, doi:10.1029/2005GL022512.

Tsunoda, R. T. (2008), Satellite traces: An ionogram signature for large-scale wave structure and a precursor for equatorial spread F, *Geophys. Res. Lett.*, *35*, L20100, doi:10.1029/2008GL035705.

Tsunoda, R. T., and B. R. White (1981), On the generation and growth of equatorial backscatter (n) plume: 1. Wave structure in the bottomside F layer, *J. Geophys. Res.*, *86*, 3610–3616.

Vadas, S. L. (2007), Horizontal and vertical propagation and dissipation of gravity waves in the thermosphere from lower atmospheric and thermospheric sources, *J. Geophys. Res.*, *112*, A06305, doi:10.1029/2006JA011845.

Vadas, S. L., and G. Crowley (2010), Sources of traveling ionospheric disturbances observed by the ionospheric TIDDBIT sounder near Wallops Island on 30 October 2007, *J. Geophys. Res.*, *115*, A07324, doi:10.1029/2009JA015053.

Zalesak, S. T., S. L. Ossakow, and P. K. Chaturvedi (1982), Nonlinear equatorial spread F: The effect of neutral winds and background conductivity, *J. Geophys. Res.*, *87*, 151–166.